# Exploring Internally Coupled Resonator's Dynamics and Spatial Variability in Metamaterials for Vibration Suppression

Alimohammadi, H.; Vassiljeva, K.; Hassan HosseinNia , S.; Petlenkov, E.

**DOI**
10.1117/12.3024067

**Publication date**
2024

**Document Version**
Final published version

**Published in**
Active and Passive Smart Structures and Integrated Systems XVIII

# Exploring Internally Coupled Resonator's Dynamics and Spatial Variability in Metamaterials for Vibration Suppression

H. Alimohammadi[a], K. Vassiljeva[b], S. H. HosseinNia[b], and E. Petlenkov[a]

[a]Department of Computer Systems, Tallinn University of Technology, Tallinn, Estonia
[b]Department of Precision and Microsystems Engineering, Delft University of Technology, Delft, The Netherlands

## ABSTRACT

Metamaterials have marked notable advancements in vibration damping and energy harvesting. However, the specific impact of internal coupled resonators, encompassing both linear and nonlinear types, has received limited attention from researchers. This study aims to delve into this underexplored area. Utilizing a distributed parameter model grounded in modal analysis, our research investigates the effects of these coupled resonators on metamaterial functionality. We particularly emphasize the influence of varying the position of attached masses and its consequent impact on the bandgap properties. Through developing theoretical and mathematical models for metastructural beams with internally coupled resonators, our approach facilitates future simulations and analyses. This investigation not only provides pivotal insights for the design and optimization of metamaterials but also underscores the possible potential of manipulating resonator properties to broaden their practical applications.

**Keywords:** Distributed parameter model, Modal analysis, Nonlinear internally coupling, Spatial variation

## 1. INTRODUCTION

Locally resonant metamaterials are engineered materials designed with unique vibrational properties that allow them to selectively amplify or dampen mechanical waves within certain frequency ranges. Through the strategic arrangement and geometry of resonators within these materials, they can control wave propagation, enabling effects such as wave trapping, vibration isolation, and wave guiding. These materials are applied in various fields, including acoustic and vibration control, energy harvesting, and advanced sensing technologies. A key feature of locally resonant metamaterials is their ability to create low-frequency bandgaps, where wave propagation is blocked, differentiating them from phononic crystals that use Bragg scattering for this purpose. This characteristic makes them particularly valuable for research in vibration attenuation and offers a broad spectrum of potential applications in related fields.

In the field of locally resonant metastructures, various methods have been identified to expand bandgaps, such as utilizing multiple periodic arrays, employing multi-degree-of-freedom local resonators, and integrating Bragg-type with resonance-type bandgaps. Techniques like internal coupling between resonators, quasi-periodic arrangements, and leveraging smart materials and actuators are underscored for their contributions to enhanced vibrational control.

The study of transverse vibrations in cantilever beams, as presented by Frank Pai et al.,[1] underlines the advantages of multi-frequency vibration absorbers in establishing effective stopbands for wave absorption. This research emphasizes the critical role of boundary conditions and the distribution of absorbers, especially significant at low frequencies.

The inclusion of mass within a system is identified as beneficial for enhancing damping, vibration control, and structural stability. The investigation conducted by Skoblar et al.[2] focuses on the effects of additional mass

Further author information: (Send correspondence to E. Petlenkov)
E. Petlenkov: E-mail: eduard.petlenkov@taltech.ee, Telephone: 1 234 567 890

Active and Passive Smart Structures and Integrated Systems XVIII, edited by Serife Tol, Guoliang Huang, Xiaopeng Li, Mostafa A. Nouh, Shima Shahab, Jinkyu Yang, Proc. of SPIE Vol. 12946, 1294614 · © 2024 SPIE · 0277-786X · doi: 10.1117/12.3024067

on the dynamic response of cantilever beams, providing insights into the vibration characteristics and overall system behavior. Piezoelectric materials' capability for energy conversion is exploited in adjusting the resonant frequency of cantilever beams, with Yuejuan Li et al.[3] offering a methodology for modifying frequency sensitivity through the strategic placement of attached masses. Magnetic actuators are highlighted for their broad frequency range and robustness. Hyunseok Song et al.[4] introduce a magneto-mechano-electric generator that features self-resonance tunability, illustrating its use in consistently powering IoT sensor systems in variable conditions. The formulation of a general mathematical model for analyzing locally resonant metastructures by Sugino et al.[5] establishes a systematic approach for predicting structure behavior and facilitating design optimization, with a particular emphasis on modal analysis to delineate bandgap properties.

The exploration of metastructures with internal coupling and nonlinear resonators is motivated by their potential to improve bandgap formation and vibration suppression. Research by Hu et al.[6] and Xia et al.[7] delves into novel designs for energy harvesting and vibration attenuation, highlighting the efficacy of alternate coupling mechanisms and the influence of excitation intensity on vibrational modes.

### 1.1 Internally coupled resonators

The subsection on internally coupled resonators delves into the advancements in metamaterial beam designs that significantly enhance energy harvesting capabilities in the low-frequency range while also marginally improving vibration suppression through the introduction of an additional band gap. Bao et al.[8] explored the enhancement of vibration suppression performance in the low-frequency region by using a locally resonant metamaterial beam coupled with horizontal springs. Their findings indicate that variables such as the number of units, damping ratio, mass, and stiffness critically influence the bandgap, leading to improved vibration suppression in locally resonant metamaterial beams.

Moreover, Hu et al.[6] introduced a modified metamaterial beam designed for dual purposes: vibration suppression and energy harvesting. This design features local resonators that are alternately coupled, with each resonator equipped with a piezoelectric element to convert vibrations into electrical energy. Furthermore, Oyelade and Oladimeji[9] presented an innovative metamaterial with a multiresonator mass-in-mass lattice system, where inner masses are interconnected by a linear spring. Their research highlighted the critical role of the additional spring and mass ratio in creating two extra bandgaps, showcasing a significant advancement over traditional multiresonator lattice systems.

Despite these developments, there has been limited research on the effects of nonlinear coupling between internal resonators within metamaterials. While comprehensive reviews like Patil et al.[10] have investigated various nonlinear characteristics of metamaterials and metastructures, there remains a gap in the focused study of nonlinear internal coupling and its potential impacts on metamaterial performance.

This study aims to bridge a significant gap in metamaterial research by focusing on the effects of nonlinear coupling between internal resonators, a topic largely overlooked despite its potential to enhance system dynamics and application efficiency. Nonlinear behaviors, intrinsic to most physical systems, can lead to improved vibration control and energy harvesting mechanisms, yet their impact remains underexplored. By investigating both linear and nonlinear internal coupling, this research seeks to uncover new insights into resonator behavior, potentially advancing metamaterial design and functionality.

Additionally, the study addresses the minimal investigation into how spatial variations in resonator properties, such as changes in attached mass positions on beam-type resonators, affect natural frequencies and bandgap characteristics. Exploring these aspects could offer novel tuning methods, optimize performance, and broaden metamaterial applications, marking a pivotal step toward mitigating production tolerances and enhancing material versatility.

## 2. DISTRIBUTED PARAMETER MODEL USING MODAL ANALYSIS

The section discusses the utilization of modal analysis in the design and optimization of mechanical locally resonant metastructures. Modal analysis is essential for identifying vibration characteristics such as natural frequencies, mode shapes, and modal damping ratios, enabling the creation of metastructures tailored for specific

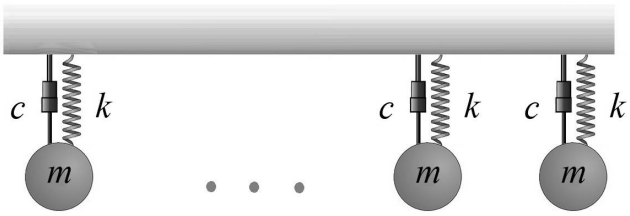


Figure 1. Example of locally resonant metastructures

wave propagation behaviors. Unlike lumped parameter models that use ordinary differential equations, distributed parameter models employ partial differential equations (PDEs) to account for the spatial distribution of physical properties within the material or structure. These models are crucial for systems where dimensions match or exceed the wavelength of wave propagation, offering insights into phenomena where spatial variations significantly influence behavior, including wave propagation, heat transfer, and fluid dynamics. Through modal analysis and the frequency determinant method, analytical models are derived to understand the dynamics of systems under base excitation and external forces, as illustrated by a typical distributed model.

Let's explore a standard distributed model that governs the oscillations of a system subjected to base excitation and external forces (refer to Figure 1). This model is formulated as a partial differential equation, drawing upon principles from Newtonian mechanics and classical references on vibration analysis.

$$\mathcal{L}w(x,t) + \mathcal{C}\frac{\partial w(x,t)}{\partial t} + \mathcal{M}\frac{\partial^2 w(x,t)}{\partial t^2} - \sum_{r=1}^{N_r}\left(k_r u_r(t) + c_r\frac{du_r(t)}{dt}\right)\delta\left(x - x_r\right) = \mathcal{F}_{b_m}(x,t) \tag{1}$$

with associated equations for the resonators:

$$m_r\frac{\partial^2 u_r(t)}{\partial t^2} + c_r\frac{\partial u_r(t)}{\partial t} + k_r u_r(t) + m_r\frac{\partial^2 w\left(x_r,t\right)}{\partial t^2} = \mathcal{F}_{b_r}(t) \tag{2}$$

The operators $\mathcal{L}, \mathcal{C}$, and $\mathcal{M}$ in the equations represent the flexural rigidity, damping, and mass distribution of the system. The main structure's transverse vibrations and those of individual resonators are denoted by $w(x,t)$ and $u_r(t)$, respectively, while $\delta\left(x - x_r\right)$ indicates the resonators' locations. $N_r$ is the number of resonators, $m_r$ their mass, $k_r$ the stiffness, and $c_r$ the damping coefficient. The mode and resonator external force is denoted by $\mathcal{F}_{b_{m,r}}(t)$, which is distributed over $D$, and the effects of the base excitation on which the beam is supported.

The boundary conditions corresponding to Eq. (1) can be expressed as

$$\mathcal{B}_i[w(x,t)] = 0, \quad i = 1, 2, \ldots, p \tag{3}$$

where $\mathcal{B}_i$ is a linear homogeneous differential operator of the order less than or equal to $2p-1$.

In many real-world structures, the concept of proportional damping often provides sufficient accuracy for estimating the natural frequencies and mode shapes of these structures.[11] Proportional damping is a distinctive kind of damping where the damping matrix is directly related to the mass and stiffness matrices. Under the assumption of proportional damping, $\mathcal{C}$ can be depicted as a blend of the mass and stiffness operators, denoted as $\mathcal{L}$ and $\mathcal{M}$.

$$\mathcal{C} = c_1\mathcal{L} + c_2\mathcal{M} \tag{4}$$

Here, $c_1$ and $c_2$ are non-negative constants determined by the physical properties of the system or through an engineering approach involving modal analysis experiments and data fitting. A benefit of employing proportional damping is the consistent mode shapes (eigenfunctions) for both the damped and undamped scenarios, and the

natural frequencies (eigenvalues) remain nearly identical.[11] As a result, the eigenfunctions $\phi_m(x)$ can be derived by solving the eigenvalue problem associated with the undamped version of Eq. (1).

$$\mathcal{L}\left[\phi_m(x)\right] = \lambda_m \mathcal{M}\left[\phi_m(x)\right], \quad m = 1, 2, ..., N_m \tag{5}$$

For a flexible structure (like a beam) with a set of resonators, the system would indeed be described by a set of coupled differential equations: one for each resonator and the flexible structure itself. Each of these components contributes to the overall dynamic behavior of the system, and they can influence each other. Since the force exerted by the resonators depends on the displacement of the structure, the mode shapes of the original structure without resonators are no longer the exact mode shapes of the full metastructure. Nevertheless, an expansion using the mode shapes of the plain structure provides significant simplification.

In the context of an Euler beam, the domain $D = [0, L]$, where the beam is assumed to be linearly elastic and homogeneous, the operators $\mathcal{L}$ and $\mathcal{M}$ can be defined as follows:

$$\mathcal{L} = EI\frac{\partial^4}{\partial x^4}, \quad \mathcal{M} = \rho A, \quad \mathcal{C} = c, \quad \mathcal{B}_1 = 1, \quad \mathcal{B}_2 = EI\frac{\partial^2}{\partial x^2}, \tag{6}$$

where $EI$ is flexural rigidity of the beam, which is the product of Young's modulus $E$ and the second moment of area $I$. $\rho$ is the density of the beam material. $A$ is the cross-sectional area of the beam.

Employing the modal expansion method, it becomes necessary for the eigenfunctions to be orthogonal to serve as the basis function for determining the solution of Eq. (1). In order to formalize the overarching principle of orthogonality, the self-adjoint (Hermitian) eigenvalue problem is outlined. For any two arbitrary eigenfunctions $\phi_m(x)$ and $\phi_n(x)$ within a one-dimensional domain, the eigenvalue problem is deemed to be self-adjoint if the following criterion is satisfied:[12]

$$\int_D \phi_m(x)\mathcal{L}\left[\phi_n(x)\right] dx = \int_D \phi_n(x)\mathcal{L}\left[\phi_m(x)\right] dx \tag{7}$$

and

$$\int_D \phi_m(x)\mathcal{M}\left[\phi_n(x)\right] dx = \int_D \phi_n(x)\mathcal{M}\left[\phi_m(x)\right] dx. \tag{8}$$

Let us now consider $\omega_m^2$ and $\omega_n^2$ as two unique eigenvalues with their corresponding eigenfunctions $\phi_m(x)$ and $\phi_n(x)$, these being the result of solving the self-adjoint eigenvalue problem. For convenience, the eigenfunctions are generally normalized with respect to $\mathcal{M}$. Consequently, the generalized condition of the orthogonality equation can be established.

$$\int_D \phi_m(x)\mathcal{M}\left[\phi_n(x)\right] dx = \delta_{mn} \tag{9}$$

and

$$\int_D \phi_m(x)\mathcal{L}\left[\phi_n(x)\right] dx = \delta_{mn}\omega_m^2 \tag{10}$$

Here, $\delta_{mn}$ is recognized as the Kronecker delta function, which yields a value of 1 when $m = n$, and maintains a value of zero in all other situations.

Under the assumption of proportional damping, the following equation is obtained:

$$\int_D \phi_m(x)\mathcal{C}\left[w_m(x)\right] dx = c_1\delta_{mn}\omega_m^2 + c_2\delta_{mn} \tag{11}$$

which can be reformulated to yield:

$$\int_D \phi_m(x)\mathcal{C}\left[w_m(x)\right] dx = \delta_{mn}2\zeta_m\omega_m \tag{12}$$

with

$$\zeta_m = \frac{1}{2\omega_m}\left(c_1\omega_m^2 + c_2\right) \tag{13}$$

Here, $\zeta_m$ denotes the damping ratio of $m$-th mode, and $c_1$ and $c_2$ are non-negative constants. Eq. (9) through to Eq. (12) constitute a set of orthonormal eigenfunctions. These eigenfunctions serve as a comprehensive basis that encapsulates the entire solution space of the eigenvalue problem.

In cases where the domain $D$ is two-dimensional, it is often more straightforward to separate the modal summation into individual summations over the two modal indices. However, it is always feasible to re-frame the double summation as a single summation over all possible combinations of the two indices. This technique, widely used in modal analysis, produces convergent solutions to the boundary value problem as formulated. The effectiveness of these solutions, undoubtedly, depends on the assumptions made during the formulation of the boundary value problem. For example, the Euler-Bernoulli beam theory might not yield accurate results at high frequencies. Furthermore, the existence of resonators in the structure creates discontinuities in the internal forces, making it necessary to use a large number of modes as a general guideline.

Using modal decomposition, the beam's deflection in the domain $D$ is expressed as a sum of modal shapes in one direction. This assumes that the behavior of the beam can be accurately represented by a finite number of modes:

$$w(x,t) = \sum_{m=1}^{N_m} \phi_m(x) z_m(t), \tag{14}$$

where $\phi_m(x)$ represents the spatial mode shape and $z_m(t)$ represents the time-dependent modal coordinate of the $m-th$ mode of the plain. These equations are to be PDEs that are used to model the dynamics of a flexible beam system integrated with discrete resonators.

Substituting the modal expansion Eq. (14) into Eq. (1), yields to:

$$\begin{aligned} &\mathcal{L}\sum_{m=1}^{N_m}\phi_m(x)z_m(t) + \mathcal{C}\frac{\partial}{\partial t}\sum_{m=1}^{N_m}\phi_m(x)z_m(t) + \mathcal{M}\frac{\partial^2}{\partial t^2}\sum_{m=1}^{N_m}\phi_m(x)z_m(t) \\ &\quad - \sum_{r=1}^{N_r}\left(k_r u_r(t) + c_r\frac{du_r(t)}{dt}\right)\delta\left(x - x_r\right) = \mathcal{F}_{b_m}(x,t) \end{aligned} \tag{15}$$

Multiplying Eq. (15) by $\phi_n(x)$ and integrating over the domain $D$, and applying the orthogonality conditions Eq. (9) to Eq. (13) of the mode shapes gives

$$\ddot{z}_m(t) + 2\zeta_m\omega_m\dot{z}_m(t) + \omega_m^2 z_m(t) - \sum_{r=1}^{N_r} m_r\omega_r^2 u_r(t)\phi_m\left(x_r\right) = \mathcal{Q}_{b_m}(x,t), \quad m = 1,2,\ldots,N_m \tag{16}$$

Similarly for resonators, substituting the modal expansion Eq. (14) into Eq. (2) yields to:

$$\ddot{u}_r(t) + 2\xi_r\omega_r\dot{u}_r(t) + \omega_r^2 u_r(t) + \sum_{m=1}^{N_m}\ddot{z}_m(t)\phi_m\left(x_r\right) = \mathcal{Q}_{b_r}(t), \quad r = 1,2,\ldots,N_r \tag{17}$$

For ease of representation, the superscript *dot* denotes the derivative with respect to time, while the superscript *prime* signifies the derivative with respect to spatial location. Each equation characterizes the dynamics of the corresponding modal coordinate or resonator displacement through a second-order ordinary differential equation. The motion is influenced by the modal or resonator parameters (natural frequencies $\omega_m$ and $\omega_r$, damping ratios

$\zeta_m$ and $\zeta_r$), the interaction between the beam modes and resonators, and the effective forces due to base excitation ($\mathcal{Q}b_m$ and $\mathcal{Q}b_r$).

The accomplishment of decoupling can be attained by executing an orthogonal transformation, which comprises pre- and post-multiplication of the mode shape matrix. This transformation process results in the diagonalization of the mass and stiffness matrices, as the eigenvectors are orthogonal to both matrices. As a consequence, a set of decoupled ordinary differential equations is derived. The normal mode method is applicable only when there is no damping or when the damping matrix is proportional, as previously assumed, implying it can be presented as a linear combination of the mass and stiffness matrices. The practice of pre- and post-multiplying the mode shape matrix with the mass and stiffness matrices is often referred to as an orthogonal transformation. When the mode shape is normalized to the mass matrix, this transformation is known as an orthonormal transformation.

By merging the basic structure depicted in Eq. (16) and the resonators represented in Eq. (17), the inertial terms of the system can be coupled, the stiffness can be decoupled, which enables further examination of the system in the frequency domain. This integration process leads to :

$$\begin{aligned}\ddot{z}_m(t) + 2\zeta_m\omega_m\dot{z}_m(t) + \omega_m^2 z_m(t) + \sum_{r=1}^{N_r} m_r\phi_m(x_r)\sum_{p=1}^{N_m}\ddot{z}_m(t)\phi_p(x_r) + \\ \sum_{r=1}^{N_r} m_r\ddot{u}_r(t)\phi_m(x_r) + 2\sum_{r=1}^{N_r} m_r\phi_m(x_r)\zeta_r\omega_r\dot{u}_r(t) = \mathcal{H}_{b_m}(x,t), \quad m = 1,2,\ldots,N_m\end{aligned} \tag{18}$$

where

$$\mathcal{H}_{b_m}(x,t) = \int_0^L \mathcal{F}_e(x,t)\phi_m(x)dx - \ddot{w}_b(t)\left(\int_0^L \mathcal{M}\phi_m(x)dx + \sum_{r=1}^{N_r} m_r\phi_m(x_r)\right) - \dot{w}_b(t)\int_0^L \mathcal{C}\phi_m(x)dx \tag{19}$$

Eqs. (17) and (18) represent a set of $N_m + N_r$ coupled second-order linear ordinary differential equations. The simultaneous solution of these equations enables the estimation of the mode shapes and resonant frequencies of the complete system, as well as the analysis of its steady-state response to harmonic excitation.

Laplace Transform facilitates the system's analysis in the frequency domain, which often proves simpler to handle algebraically than the original time-domain equations. Therefore, applying the Laplace Transform to Eqs. (17) and (18), under the assumption of zero initial conditions, results in:

$$U_r(s) = \frac{\mathcal{Q}_{b_r}(s) - \sum_{m=1}^{N_m} s^2 Z_m(s)\phi_m(x_r)}{s^2 + 2\xi_r\omega_r s + \omega_r^2} \tag{20}$$

$$\begin{aligned}s^2 Z_m(s) + 2\zeta_m\omega_m s Z_m(s) + \omega_m^2 Z_m(s) + \sum_{r=1}^{N_r} m_r\phi_m(x_r)\sum_{p=1}^{N_m} s^2 Z_p(s)\phi_p(x_r) + \\ \sum_{r=1}^{N_r} m_r s^2 U_r(s)\phi_m(x_r) + 2\sum_{r=1}^{N_r} m_r\phi_m(x_r)\zeta_r\omega_r s U_r(s) = H_{b_m}(s), \quad m = 1,2,\ldots,N_m\end{aligned} \tag{21}$$

Here, $Z_m(s)$ and $U_r(s)$ symbolize the Laplace Transforms of the modal coordinates and the resonator displacements, respectively. For further analytical understanding, the Laplace Transform is applied to Eq. (17), following the assumptions made in:[5]

$$\sum_{r=1}^{N_r} m_r\phi_m(x_r)\phi_m(x_r) \approx \mu, \quad Q_{b_r}(s) = 0 \tag{22}$$

where $\mu$ represents the mass ratio, which is the sum of the resonators' mass to the mass of the plain beam.

Applying these assumptions results in the following expression:

$$U_r(s) = -\frac{s^2}{s^2 + 2\zeta_r\omega_r s + \omega_r^2} \sum_{r=1}^{N_r} Z_m(s)\phi_m\left(x_r\right), \quad r = 1, 2, \ldots, N_r \tag{23}$$

Applying the Laplace transform to Eq. (16) and substituting from Eq. (23) gives the following result:

$$\frac{Z_m(s)}{Q_{b_m}(s)} = \frac{1}{s^2\left(1 + \frac{\mu\omega_r^2}{s^2+2\zeta_r\omega_r s+\omega_r^2}\right) + 2\zeta_m\omega_m s + \omega_m^2} \quad m = 1, 2, \ldots, N_m \tag{24}$$

Eq. (24) reveals that the presence of resonators brings about a frequency-dependent mass term. Assuming an infinite number of resonators, which results in continuous displacements throughout the space, similar simplifications can be made for the resonator displacements. Substituting Eq. (24) into Eq. (23) and replacing the discrete variable $x_r$ with the continuous variable $x$, the following equation can be derived:

$$U_r(s) = -\frac{s^2}{s^2 + 2\zeta_r\omega_r s + \omega_r^2} \sum_{m=1}^{N_m} \phi_m\left(x_r\right) \frac{Q_{b_m}(s)}{s^2\left(1 + \frac{\mu\omega_r^2}{s^2+2\zeta_r\omega_r s+\omega_r^2}\right) + 2\zeta_m\omega_m s + \omega_m^2} \tag{25}$$

This provides a continuous equation for the motion $U_r(s)$ of the resonators along the beam, expressed in terms of the modal force inputs $Q_{b_m}(s)$.

The resonators' displacement can now be expressed as a linear combination of the plain structure's mode shapes in Laplace form:

$$U_r(s) = \sum_{m=1}^{N_m} \Psi_m(s)\phi_m(x) \tag{26}$$

Equation (26) can be associated with Eq. (25) by identifying the modal coordinates within the Laplace domain, given by $\Psi_m(s)$, as follows:

$$\frac{\Psi_m(s)}{Q_{b_m}(s)} = -\frac{s^2}{\left[s^2 + 2\zeta_r\omega_r s + \omega_r^2\right]\left[s^2\left(1 + \frac{\mu\omega_r^2}{s^2+2\zeta_r\omega_r s+\omega_r^2}\right) + 2\zeta_m\omega_m s + \omega_m^2\right]}, \quad m = 1, 2, \ldots, N_m \tag{27}$$

The transfer function depicted in Eq. (27) elucidates the relationship between the modal force $Q_{b_m}(s)$ and the modal coordinate $\Psi_m(s)$. It provides insight into the system's dynamics. The poles of this function, where the function's values reach their maximum, correspond to the system's resonant frequencies.

Investigating the system stability further, as outlined by Eq. (24), demands an exploration of the system poles. As shown in Figure 2, the impact of resonators and damping on the frequency response and stability of the system. The introduction of the resonator results in frequency splitting, manifesting as a distinct frequency bandgap in the Bode plot. The exhibited splitting, regardless of the system's damping characteristics, underscores the substantial impact of the resonators. They shape the system's behavior by engaging with the intrinsic dynamics of the beam, thereby underscoring the importance of considering resonator influence in the modeling and analysis of such systems. Damping emerges as a crucial element in ensuring system stability. In the absence of damping, poles reside on the imaginary axis or the right half of the complex plane, indicating marginal stability or instability. However, with the inclusion of damping, these poles effectively shift to the left half of the complex plane, denoting system stability as seen in Root Locus plot in Figure 2. This pivotal transition is evident in various analyses, such as the Lyapunov stability criterion, reinforcing the fundamental role of damping in stabilizing the system and optimizing its performance. Moreover, in the damped system, both the beam and

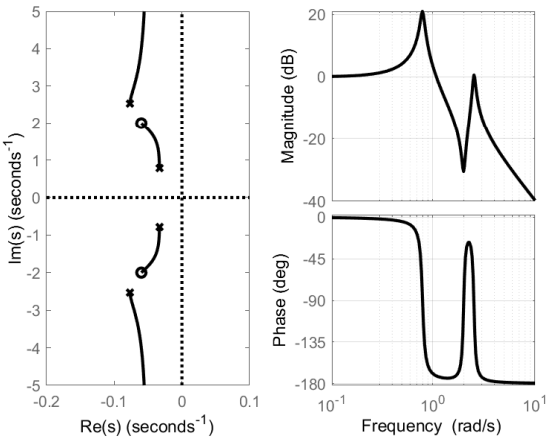


Figure 2. Root Locus and Bode plot analysis of Eq.(24) with parameters $\omega_m = 1$, $\omega_r = 2$, $\zeta_m = 0.05$, $\zeta_r = 0.03$, $\mu = 0.5$.


Figure 3. Locally resonant metastructures with internally coupled resonators

resonator's resonant frequencies are slightly lower than their undamped counterparts. This reduction in resonant frequencies results in smaller peaks in the frequency response, while damping also introduces a phase shift in the system's frequency response, further altering its characteristics. These effects underscore the importance of understanding and considering damping in system design and control strategies, as it not only ensures stability but also influences the magnitude and phase aspects of the system's response. It is clearly depicted from Root Locus in Figure 2 that there are no poles within the locally resonant bandgap zone, which falls within the frequency range of $\omega_r < \mathrm{Im}(s) < \omega_r\sqrt{1+\mu}$.

Further investigation of the effects of mass ratio, $\mu$, and root locus interpretation of the bandgap, taking into account the neglect and exclusion of effects of base excitation on resonators ($Q_{b_r}$), and for undamped system can be found in the work by Sugino et al.[5]

## 3. INTERNALLY COUPLED RESONATORS MODELING

### 3.1 Linear system

By incorporating a linear coupling term, $k_c$, into the resonators depicted in Fig. 3, the system transforms into a connected duo of resonators. This alteration leads to a scenario where the movements of the resonators are intertwined rather than independent. In particular, the motion of one resonator directly affects the motion of its counterpart, fostering a dynamic interplay. The energy stemming from this coupling is captured by the coupling potential energy, where each resonator pair (1 and 2, 3 and 4, 5 and 6, etc.) constitutes a system characterized by two degrees of freedom.

$$V_c(t) = \frac{1}{2}k_c\left(u_{r_1}(t) - u_{r_2}(t) + w\left(x_{r_1}, t\right) - w\left(x_{r_2}, t\right)\right)^2 \tag{28}$$

The equations governing the coupled resonator system are derived as follows:

$$\ddot{z}_m(t) + 2\zeta_m\omega_m\dot{z}_m(t) + \omega_m^2 z_m(t) - \sum_{r=1}^{N_r/2}\left(m_{2r-1}\omega_{2r-1}^2 u_{2r-1}(t)\phi_m\left(x_{2r-1}\right) + m_{2r}\omega_{2r}^2 u_{2r}(t)\phi_m\left(x_{2r}\right)\right) = \mathcal{Q}_{b_m}, \quad m = 1, 2, \ldots, N_m, \text{ and } N_r \in 2\mathbb{N} \tag{29}$$

Meanwhile, the equation for the resonators is given by:

$$\ddot{u}_{2r-1}(t) + 2\xi_{2r-1}\omega_{2r-1}\dot{u}_{2r-1}(t) + \omega_{2r-1}^2 u_{2r-1}(t) + \sum_{m=1}^{N_m}\ddot{z}_m(t)\phi_m\left(x_{2r-1}\right) + \beta\frac{k_c}{m_{2r-1}} = \mathcal{Q}_{b_{2r-1}}, \quad r = 1, 2, \ldots, N_r/2 \tag{30}$$

$$\ddot{u}_{2r}(t) + 2\xi_{2r}\omega_{2r}\dot{u}_{2r}(t) + \omega_{2r}^2 u_{2r}(t) + \sum_{m=1}^{N_m}\ddot{z}_m(t)\phi_m\left(x_{2r}\right) - \beta\frac{k_c}{m_{2r}} = \mathcal{Q}_{b_{2r}}, \quad r = 1, 2, \ldots, N_r/2 \tag{31}$$

where

$$\beta = u_{2r-1}(t) - u_{2r}(t) + \sum_{m=1}^{N_m}\ddot{z}_m(t)\phi_m\left(x_{2r-1}\right) - \sum_{m=1}^{N_m}\ddot{z}_m(t)\phi_m\left(x_{2r}\right) \tag{32}$$

These equations delineate the fundamental dynamics of the beam along with the system of internally linearly coupled resonators.

### 3.2 Nonlinear system

In the case of a nonlinear coupling, the nature of interaction between the resonators becomes more intricate and more interesting dynamics can emerge. This nonlinearity could arise from various sources such as mechanical, magnetic, or electrical interactions. The equations governing the system behavior in this case would contain nonlinear terms and could potentially give rise to phenomena like bifurcations, chaos, or complex oscillatory behaviors. The analysis and understanding of such systems often requires advanced mathematical techniques and may involve numerical simulations. The exact form of the equations would depend on the specific form of nonlinearity in the coupling.

In the case of bistable nonlinearity (quadratic and quartic terms), the energy associated with this coupling can be formed as:

$$V_c(t) = \frac{1}{2}k_{c_1}\left(u_{r_1}(t) - u_{r_2}(t) + w(x_{r_1}, t) - w(x_{r_2}, t)\right)^2 + \frac{1}{4}k_{c_2}\left(u_{r_1}(t) - u_{r_2}(t) + w(x_{r_1}, t) - w(x_{r_2}, t)\right)^4 \tag{33}$$

The quadratic term represents the linear coupling between the resonators, while the quartic term introduces an additional nonlinearity that leads to bistability for negative $k_{c_1}$. The quartic term can create a double-well potential energy landscape, allowing for the presence of two stable equilibrium positions for the resonators. The dynamic of resonators forms to:

$$\ddot{u}_{2r-1}(t) + 2\xi_{2r-1}\omega_{2r-1}\dot{u}_{2r-1}(t) + \omega_{2r-1}^2 u_{2r-1}(t) + \sum_{m=1}^{N_m} \ddot{z}_m(t)\phi_m\left(x_{2r-1}\right) + \frac{k_{c_1}\beta}{m_{2r-1}} + \frac{k_{c_2}\beta^3}{m_{2r-1}} = \mathcal{Q}_{b_{2r-1}}, \quad r = 1, 2, \ldots, N_r/2 \tag{34}$$

$$\ddot{u}_{2r}(t) + 2\xi_{2r}\omega_{2r}\dot{u}_{2r}(t) + \omega_{2r}^2 u_{2r}(t) + \sum_{m=1}^{N_m} \ddot{z}_m(t)\phi_m\left(x_{2r}\right) - \frac{k_{c_1}\beta}{m_{2r}} - \frac{k_{c_2}\beta^3}{m_{2r}} = \mathcal{Q}_{b_{2r}}, \quad r = 1, 2, \ldots, N_r/2 \tag{35}$$

Equations (29) to (35) present a more comprehensive formulation that is compatible with the approach taken in[5] when neglecting the coupling effects, and damping of the structure and resonators. Moreover, this equation advances the previous work by incorporating a modal representation for both the structure and resonators, a detail overlooked in reference,[5] thereby providing a more complete representation of the system.

## 4. DISPERSION ANALYSIS AND MODEL VALIDATION OF INTERNALLY COUPLED RESONATORS BY PLANE WAVE EXPANSION METHOD

### Linear system

The Plane Wave Expansion (PWE) method is commonly used for analyzing the propagation of waves in periodic structures, and provides valuable insights into the behavior of these waves, facilitating the design and optimization of these periodic structures for a wide range of applications, such as vibration suppression and energy harvesting.[13,14]

Let's define the transverse displacement of metastructure and resonators with linear internally coupled in absolute coordinate as $W_t(x,t) = \hat{W}_t e^{i(G_n x - \omega t)}$ for the beam, $z_{r_1}(t) = \hat{z}_{r_1} e^{i(\omega t)}$ for the first resonator, and $z_{r_2}(t) = \hat{z}_{r_2} e^{i(\omega t)}$ for the second resonator.

$$EIG_n^4 \hat{W}_t\left(G_n\right) - \rho A\omega^2 \hat{W}_t\left(G_n\right) + k_{r_1}\hat{W}_t\left(G_n\right) + k_{r_2}\hat{W}_t\left(G_n\right) - k_{r_1}\hat{z}_{r_1} - k_{r_2}\hat{z}_{r_2} = 0 \tag{36}$$

$$-k_{r_1}\hat{W}_t\left(G_n\right) + k_c\hat{z}_{r_1} - k_c\hat{z}_{r2} + k_{r_1}\hat{z}_{r_1} - m_{r_1}\omega^2\hat{z}_{r_1} = 0 \tag{37}$$

$$-k_{r_2}\hat{W}_t\left(G_n\right) - k_c\hat{z}_{r_1} + k_c\hat{z}_{r2} + k_{r_2}\hat{z}_{r_2} - m_{r_2}\omega^2\hat{z}_{r_2} = 0 \tag{38}$$

The equations capture the interactions within a metastructure, highlighting the dynamics between the main beam and resonators via coupling constants and mass effects, crucial for understanding wave propagation. The internal coupling term, $k_c$, is uniquely present in the resonators' equations, indicating that the coupling directly links the two resonators, rather than connecting them with the main beam. This setup points to a direct interaction between resonators, although it implies that forces resultant from this coupling can still transfer to the main beam, affecting its overall dynamics.

The dispersion relation is obtained by imposing periodic boundary conditions and seeking non-trivial solutions. In one-direction transformation the relation between the frequency $\omega$ and the wavevector $G_n$ is achieved by multiplying the amplitude of the variable by a complex exponential function $\exp(i(G_n x - \omega t))$, which can be written in the form:

$$C_1\omega^6 + C_2\omega^4 + C_3\omega^2 + C_4 = 0 \tag{39}$$

where:

$$
\begin{aligned}
C_1 &= -Am_{r_1}m_{r_2}\rho, \\
C_2 &= m_{r_1}m_{r_2}\left(EIG_n^4 + k_{r_1} + k_{r_2}\right) + A\rho\left(m_{r_1} + m_{r_2}\right)k_c + A\rho m_{r_2}k_{r_1} + A\rho m_{r_1}k_{r_2}, \\
C_3 &= -\left(k_c\left(m_{r_1} + m_{r_2}\right)\left(k_{r_1} + k_{r_2}\right) + A\rho\left(k_{r_1}k_{r_2} + k_c\left(k_{r_1} + k_{r_2}\right)\right) + EIG_n^4 m_{r_1}m_{r_2}\left(k_c + k_{r_2} + k_{r_1}\right)\right), \\
C_4 &= EIG_n^4\left(k_c\left(k_{r_1} + k_{r_2}\right) + k_{r_1}k_{r_2}\right).
\end{aligned}
\tag{40}
$$

**Nonlinear system**

$$
EIG_n^4\hat{W}_t\left(G_n\right) - \rho A\omega^2\hat{W}_t\left(G_n\right) + k_{r_1}\hat{W}_t\left(G_n\right) + k_{r_2}\hat{W}_t\left(G_n\right) - k_{r_1}\hat{z}_{r_1} - k_{r_2}\hat{z}_{r_2} = 0 \tag{41}
$$

The first and second nonlinear internally coupled resonators are:

$$
-k_{r_1}\hat{W}_t\left(G_n\right) + k_{c_1}\hat{z}_{r_1} - k_{c_1}\hat{z}_{r_2} + k_{r_1}\hat{z}_{r_1} + k_{c_2}\hat{z}_{r_1}^3 - k_{c_2}\hat{z}_{r_2}^3 - m_{r_1}\omega^2\hat{z}_{r_1} + 3k_{c_2}\hat{z}_{r_1}\hat{z}_{r_2}^2 - 3k_{c_2}\hat{z}_{r_1}^2\hat{z}_{r_2} = 0 \tag{42}
$$

$$
-k_{r_2}\hat{W}_t\left(G_n\right) - k_{c_1}\hat{z}_{r_1} + k_{c_1}\hat{z}_{r_2} + k_{r_2}\hat{z}_{r_2} - k_{c_2}\hat{z}_{r_1}^3 + k_{c_2}\hat{z}_{r_2}^3 - m_{r_2}\omega^2\hat{z}_{r_2} - 3k_{c_2}\hat{z}_{r_1}\hat{z}_{r_2}^2 + 3k_{c_2}\hat{z}_{r_1}^2\hat{z}_{r_2} = 0 \tag{43}
$$

Due to the system's nonlinearity, the utilization of the determinant of the matrix approach failed. These transforms are computed numerically.

## 5. NUMERICAL STUDY

The complexity of such equations is increased due to the coupling induced by resonators, which obstructs a straightforward analytical solution for $Z_m(s)$. Therefore, numerical methods become necessary to determine the system response. In cases of non-linear equations which may not have closed-form solutions, state-space representation proves advantageous. This method involves casting the system in matrix form, complete with an associated vector $[Z_m(s), U_r(s)]$ of size $[N_m + N_r]$. Subsequently, numerical methods like the Newton-Raphson algorithm can assist in computing the Fourier series expansion coefficients. However, when the Newton-Raphson method fails to converge, the Runge-Kutta method served as an effective alternative, especially in situations where the system exhibits high nonlinearity and a large number of degrees of freedom.

The geometric and material properties of the investigated rectangular beam are detailed in Table 1. The attached mass $m_a$ is positioned at various locations along the resonator, with their distances ranging from 20 to 57.3 mm. The coupling spring constants are $k_c$ and $k_{c_1}$, with a second nonlinear coupling constant $k_{c_2}$ being studied, providing a basis for further analysis and simulations.

Table 1. Geometric and material properties for the studied rectangular beam

| Parameter | Value | Parameter | Value |
|---|---|---|---|
| $L_m$ | 0.3 m | $m_r$ | 5.9 g |
| $w_m$ | 25 mm | $k_r$ | 374 N/m |
| $h_m$ | 3 mm | $\zeta_r$ | 0.003 |
| $\rho_m$ | 2700 kg/m$^3$ | $N_r$ | 8 |
| $E_m$ | 70 GP | $m_a$ | 3.8 g |
| $\zeta_m$ | 0.01 | $k_{c_1}$ | $-37.4$ N/m |
| $N_m$ | 10 | $k_{c_2}$ | 102 N/m$^3$ |
| $k_c$ | 374 N/m | $\delta$ | [20...57.3] mm |

Fig. 4 presents the simulation of the linear transmissibility characteristics of a clamped-free beam without any attachments, referred to in this context as a plain beam. Notably, the distinct separation of the first three

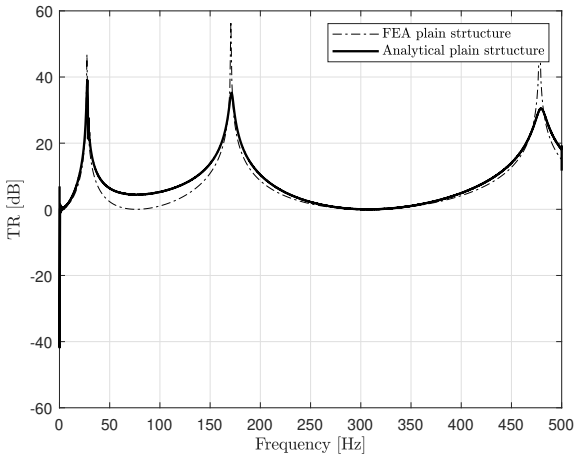


Figure 4. Validation of studies plain structure

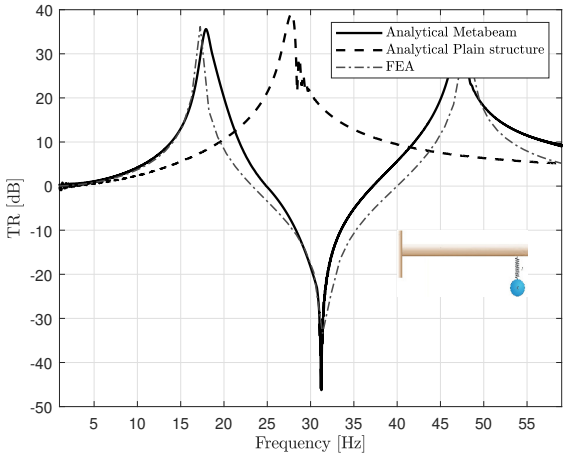


Figure 5. Bandgap formation and anti-resonance phenomena in a vibration absorber structure with an additional resonator

modes can be clearly observed. The outcomes from this simulation align well with the results obtained from finite element analysis (FEA) for the plain beam, underscoring the validity of the simulation approach. The parameters for this study were carefully selected to mirror the conditions in the FEA model, thus boosting the validity of the simulation.

Fig. 5 demonstrates the impact of introducing an additional resonator into the system. This addition induces the formation of a bandgap, mimicking the attributes of a traditional vibration absorber structure. Consequently, an anti-resonance event is noted around the resonator's natural frequency. This occurrence is instrumental in attenuating specific frequencies in the vibration spectrum, reflecting the response of a single resonator, comparable to a classical vibration absorber structure. The figure depicts the resonator at the end of the beam, with the simulated results exhibiting a high degree of agreement with the FEA outcomes. This concurrence validates the precision of the simulation and the reliability of the modeling assumptions employed. The dash-solid line in Fig. 5 corresponds to the case of a plain beam without an attached local resonator. This case provides a stark contrast, as no bandgap phenomenon is observed, highlighting the pivotal role local oscillators play in the system's vibrational properties. Such insights are crucial when it comes to designing systems to control and manipulate desired vibrational behaviors.

Fig. 6 demonstrates the bandgap extracted from the plane wave expansion dispersion analysis for a conventional metamaterial. The displayed curve outlines the relationship between wave frequency and wavenumber,

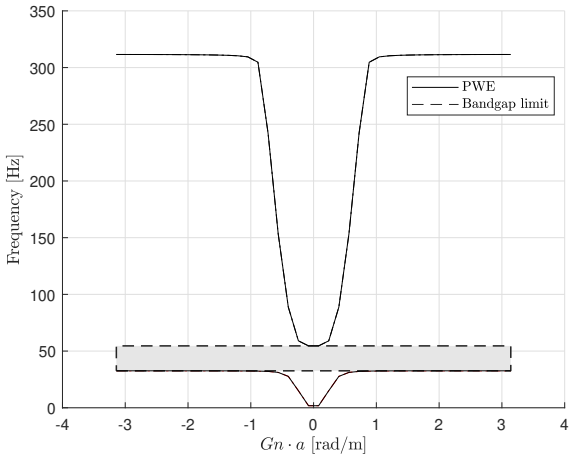


Figure 6. Dispersion curves computed using the plane wave expansion method for target frequency $f_t$=31.2 Hz

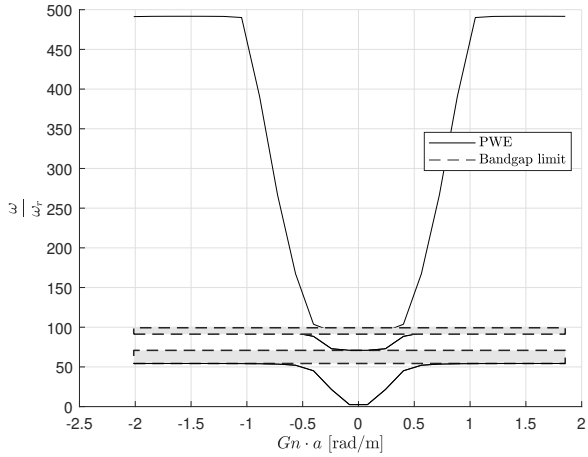


Figure 7. Dispersion curve of internally coupled metamaterial beam using the plane wave expansion method for target frequency $k_c = k_r$ and $f_t$=31.2 Hz.

providing insight into the spatial variation of the wave within the structure. Based on the design parameters, the curve reveals that wave propagation occurs within a frequency range of 31.5 Hz to 52.4 Hz. The figure identifies the presence of bandgaps within this range, where specific frequencies are prevented from propagating through the structure. The target mode is selected at $f_r$=31.2 Hz. This mode signifies frequency ranges where the wave propagation is strongly influenced by local resonance, leading to the opening of a bandgap in the out-plane phase. Understanding this interaction between local resonance and wave propagation provides critical information for the effective design and application of metamaterials.

Fig. 7 illustrates the bandgap derived from the plane wave expansion dispersion analysis outlined in Eq. (41). This figure highlights the first bandgap (indicated by the shaded area), which aligns with that of the conventional metamaterial beam in Fig. 6. Furthermore, a second, narrower bandgap is observed at a slightly higher frequency range. Notably, this additional bandgap is a result of internal coupling within the metamaterial structure. The presence of this second bandgap, brought about by internal coupling, could profoundly impact the wave propagation characteristics and subsequent design strategies of such metamaterials.

The bandgap depicted in Fig. 8 aligns well with the plane wave expansion dispersion analysis presented in Fig. 6 and Fig. 7. This consistency lends credence to the analytical approach and validates the findings of the study. Compared to Fig. 5, a significant observation is that the width of the bandgap expands with

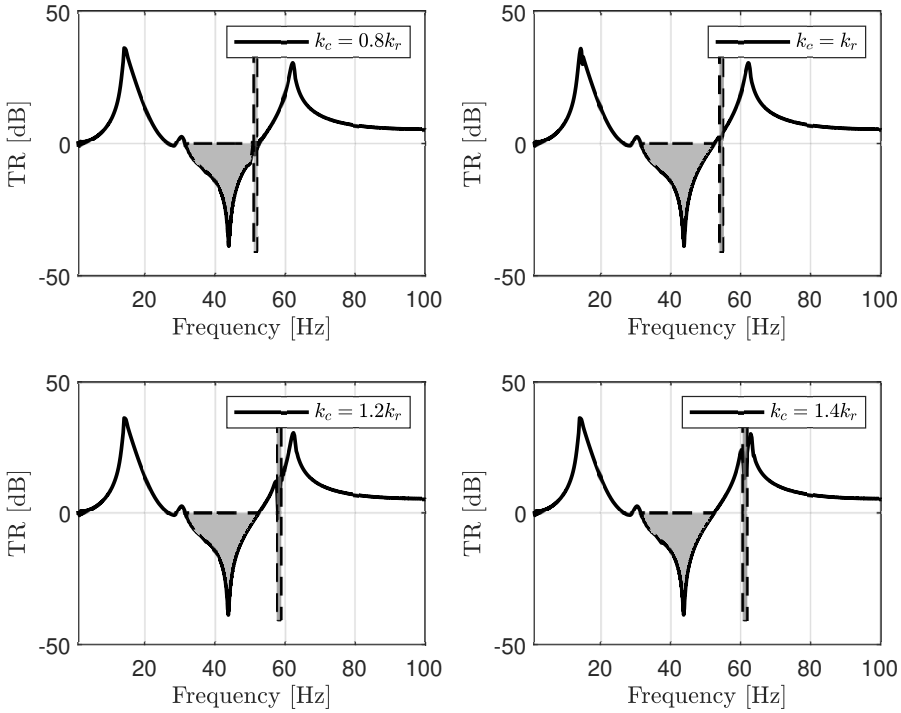


Figure 8. Transmittance of internally linear coupled $N_r$=8 resonators metamaterial beam for different $k_c/k_r$ ratios: (a) $k_c = 0.8k_r$, (b) $k_c = k_r$, (c) $k_c = 1.2k_r$, (d) $k_c = 1.4k_r$.

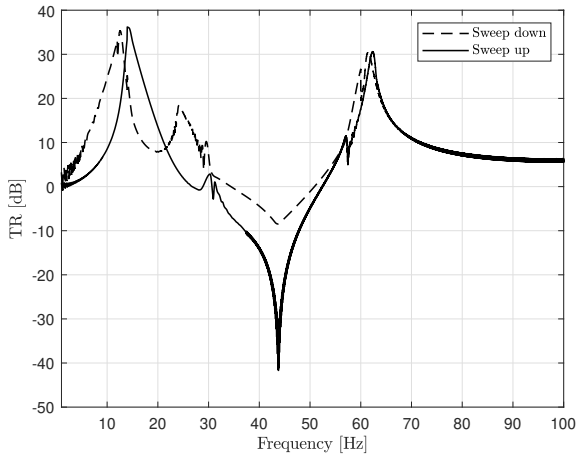


Figure 9. Transmittance of internally nonlinear coupled metamaterial beam with $N_r$=8 resonators, $k_{c_1} = 0.1k_r$ and $k_{c_2} = 0.27k_r$

the increase in the number of resonators. This expansion enhances vibration suppression, indicating that the incorporation of more resonators could lead to improved vibration control in such structures. Interestingly, it's found that an increase in the coupling spring stiffness ($k_c$) does not affect the first bandgap. On the other hand, the position of the second bandgap migrates towards higher frequencies, and its width fluctuates. However, given the relative narrowness of the second bandgap when compared to the first, alterations in its width, either increasing or decreasing, are not significantly noticeable. This suggests that changes in coupling spring stiffness may not substantially affect the overall system behavior via the width of the second bandgap.

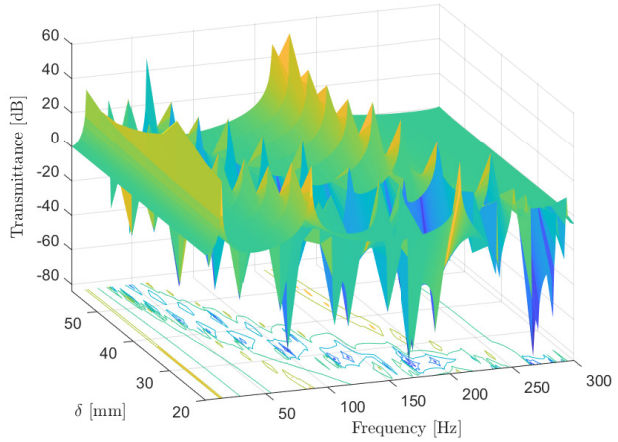


Figure 10. The transmittance pattern evolution in response to the variation of $\delta$

Fig. 9 presents the behavior of nonlinear coupled resonators, the parameters of which are selected to mirror the behavior of linear coupled resonators. As the figure depicts, the bandgap created during the frequency sweep-up matches that of the linear case. However, during the sweep-down process, the bandgap behavior diverges due to the nonlinearity of the coupled spring, resulting in a narrower bandgap compared to the linear or sweep-up frequency operation. A significant observation from the figure is the notable reduction of the first side peak around 15 Hz, accompanied by a visible softening behavior exhibited on the second side peak. These findings underline the substantial influence of nonlinearity on the vibrational behavior of the coupled resonators. Interestingly, no remarkable increase in the bandgap is observed in this case, despite the introduced nonlinearity. This observation could have significant implications for the design and control of such systems with selected parameters.

Given these observations, it is valuable to further explore nonlinear dynamics through analyses like bifurcation, chaos theory, Lyapunov exponents, or investigations into regimes far removed from linear or stable conditions. Extending this work into more complex nonlinear analyses could unveil deeper insights into the behavior and control of nonlinear coupled resonator systems, potentially leading to advanced applications and optimization techniques for managing vibrational phenomena.

## Impact of Variations in Resonator Natural Frequencies on Bandgap Characteristics

This section delves into the influence of variations in resonator natural frequencies on resonant bandgap edge frequencies. Theoretical frameworks frequently assume identical target frequency $\omega_t$ for all resonators. However, real-world resonators exhibit small variations, inevitably resulting from manufacturing inconsistencies, the distinct interfaces connecting resonators to the primary structure, and other factors. Notably, apart from these unavoidable minor variations, it is possible to intentionally adjust $\omega_t$. Such tuning of the structure enables operation within different frequency ranges, a capability crucial for broader real-world applications such as in heavy-duty machinery. This tunability presents a solution to the limitations of piezoelectric metamaterials, whose applicability is otherwise constrained. Furthermore, the location of the attached mass ($\delta$) can be varied, resulting in changes to the resonator's natural frequency due to adjustment in the effective stiffness. This ability to individually and distinctly alter each resonator's natural frequency introduces a new dimension of tunability to the system. Consequently, this approach can potentially circumvent the performance issues commonly associated with graded metamaterials, as noted in recent studies.[15,16]

In Fig. 10, the transmittance pattern evolution of a metastructural beam equipped with eight resonators is depicted in response to the variation of $\delta$, which represents the position of the attached mass. The parameters for these resonators can be referred to in Table 1. The graph displays a frequency range from 0 to 300 Hz, concurrent with the alteration in the attached mass position $\delta$ from 20 mm to 57.3 mm. The value of $\delta$ effectively quantifies

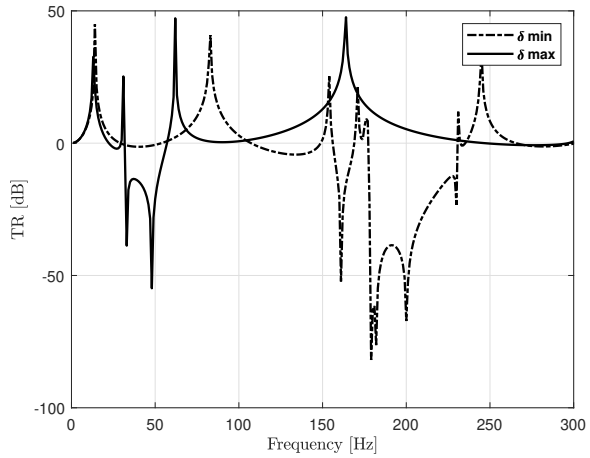


Figure 11. Effects of attached mass position on resonator natural frequencies and bandgap characteristics: comparing maximum and minimum $\delta$ scenarios

the location of the attached mass along the beam-type resonator. As $\delta$ decreases, indicating the mass is closer to the base of the resonator, a resulting increase in resonator stiffness is observed. This further escalates the resonator's natural frequency, $\omega_r$.

A key observation from the plot in Fig. 10 is that the bandgap shrinks as $\delta$ increases. This suggests that there is a maximum allowable variation in $\delta$. Moreover, the impact of $\delta$ on the width of the bandgap is of paramount importance, as visualized in Fig. 11. An attached mass moving towards the resonator's tip (an increase in $\delta$) results in a narrower bandgap. Conversely, if the mass is attached farther from the tip (a decrease in $\delta$), a broader bandgap is achieved. These insights highlight the crucial role of the attached mass position in enhancing the performance of a metastructural beam. They also propose an exciting possibility of manipulating both the central frequency and width of the bandgap by finely adjusting the location of the attached mass on each resonator.

## 6. CONCLUSION

In conclusion, the research outlined provides an expansive theoretical insight into bandgap generation within internally coupled, locally resonant metastructures. By investigating both linear and nonlinear coupled resonators, this work sheds light on the significant impact of varying resonator properties, notably the natural frequency variation of resonators and the stiffness of coupling springs. This study also unveils the substantial effect of the position of an attached mass on resonators, which dictates the natural frequency and thus governs the central frequency and width of the bandgap.

While the number of resonators can result in a wider bandgap, the impact of the stiffness of the coupling spring on the first bandgap is negligible. However, it induces a shift in the second bandgap towards higher frequencies, while also causing fluctuations in its width. Additionally, in the context of nonlinear coupled resonators, unique bandgap formation patterns were observed during sweep-up and sweep-down frequency operations, which can be attributed to the inherent nonlinearity present.

This study further examined the effects of the position of an attached mass on the natural frequency and bandgap characteristics of a cantilevered beam, highlighting a promising avenue for system tunability. While these findings offer a critical leap towards comprehensive knowledge of bandgap generation in metamaterials, it is important to note that these conclusions are bound by the assumptions of the theoretical model used. Empirical validation through future experimental studies is thus highly recommended to confirm these findings' real-world application viability.

Furthermore, the study's findings highlight the potential of metamaterials compared to conventional piezoelectric devices. The ability to finely adjust bandgap characteristics and manipulate wave propagation properties

within these metastructures offers superior vibration suppression, benefiting the maintenance and performance of various machinery, in particular heavy-duty machinery. Additionally, the design flexibility and tunability of these metastructures enhance their potential for efficient energy harvesting applications, contributing to sustainability and cost-effectiveness. By establishing a strong foundation for further exploration and optimization of metamaterial parameters, this research opens doors for broader practical applications of these innovative structures.

## Acknowledgments

This paper is supported by the European Union's HORIZON Research and Innovation Programme under grant agreement No 101120657, project ENFIELD (European Lighthouse to Manifest Trustworthy and Green AI). It was also supported by the Estonian Research Council grant PRG658.

## REFERENCES

[1] Pai, P. F., "Metamaterial-based broadband elastic wave absorber," *Journal of intelligent material systems and structures* **21**(5), 517–528 (2010).

[2] Skoblar, A., Žigulić, R., Braut, S., and Blažević, S., "Dynamic response to harmonic transverse excitation of cantilever euler-bernoulli beam carrying a point mass," *FME Transactions* **45**(3), 367–373 (2017).

[3] Li, Y., Hou, X., Qi, W., Wang, Q., and Zhang, X., "Modeling and analysis of multiple attached masses tuning a piezoelectric cantilever beam resonant frequency," *Shock and Vibration* **2020**, 1–12 (2020).

[4] Song, H., Hwang, G.-T., Ryu, J., and Choi, H., "Stable output performance generated from a magneto-mechano-electric generator having self-resonance tunability with a movable proof mass," *Nano Energy* **101**, 107607 (2022).

[5] Sugino, C., Xia, Y., Leadenham, S., Ruzzene, M., and Erturk, A., "A general theory for bandgap estimation in locally resonant metastructures," *Journal of Sound and Vibration* **406**, 104–123 (2017).

[6] Hu, G., Tang, L., and Das, R., "Internally coupled metamaterial beam for simultaneous vibration suppression and low frequency energy harvesting," *Journal of Applied Physics* **123**(5) (2018).

[7] Xia, Y., Erturk, A., and Ruzzene, M., "Topological edge states in quasiperiodic locally resonant metastructures," *Physical Review Applied* **13**(1), 014023 (2020).

[8] Bao, H., Wu, C., Zheng, W., and Yan, B., "Vibration bandgap of a locally resonant beam considering horizontal springs," *Journal of Vibration and Control* **28**(3-4), 452–464 (2022).

[9] Oyelade, A. O. and Oladimeji, O. J., "Coupled multiresonators acoustic metamaterial for vibration suppression in civil engineering structures," *Forces in Mechanics* **5**, 100052 (2021).

[10] Patil, G. U. and Matlack, K. H., "Review of exploiting nonlinearity in phononic materials to enable nonlinear wave responses," *Acta Mechanica* **233**(1), 1–46 (2022).

[11] Hansen, C., Snyder, S., Qiu, X., Brooks, L., and Moreau, D., [*Active control of noise and vibration*], CRC press (2012).

[12] Rao, S. S., [*Vibration of continuous systems*], John Wiley & Sons (2019).

[13] Li, F.-L., Zhang, C., and Wang, Y.-S., "Band structure analysis of phononic crystals with imperfect interface layers by the bem," *Engineering Analysis with Boundary Elements* **131**, 240–257 (2021).

[14] Lei, L., Miao, L., Zheng, H., Wu, P., and Lu, M., "Band gap extending of locally resonant phononic crystal with outward hierarchical structure," *Applied Physics A* **128**(6), 492 (2022).

[15] Zhao, B., Thomsen, H. R., De Ponti, J. M., Riva, E., Van Damme, B., Bergamini, A., Chatzi, E., and Colombi, A., "A graded metamaterial for broadband and high-capability piezoelectric energy harvesting," *Energy Conversion and Management* **269**, 116056 (2022).

[16] Hu, G., Austin, A. C., Sorokin, V., and Tang, L., "Metamaterial beam with graded local resonators for broadband vibration suppression," *Mechanical Systems and Signal Processing* **146**, 106982 (2021).